Defect equilibria in undoped a-Si:H

R. A. Street and K. Winer
Xerox Corporation, Palo Alto Research Center, Palo Alto, California 94304
(Received 21 February 1989)

Experimental and theoretical studies of the thermal equilibrium defect density in undoped a-Si:H are reported. The defect density measured by electron-spin resonance increases with temperature with an activation energy of 0.15–0.2 eV. The equilibration time is activated with an energy of about 1.5 eV, and the shape of the decay follows a stretched exponential, as in doped a-Si:H. The experiments confirm that defect equilibration occurs over a range of temperatures and sample deposition conditions. The relaxation time depends on the growth conditions, and the thermal defects are shown to anneal more slowly than optically induced defects. The temperature dependence of the thermodynamic equilibrium defect density is calculated, based on the weak-bond–dangling-bond conversion model. Four specific defect reactions are analyzed, two of which involve the motion of bonded hydrogen. The defect density is sensitive to the details of the model because of entropy effects. The experimental data agree well with the analysis, but do not conclusively distinguish between the different possible defect reactions because of uncertainties in the parameters of the model. The different annealing rates of thermal and optical defects are accounted for by relating the distributions of hydrogen-bonding energies, the defect-formation energies, and the valence-band-tail states. It is proposed that the time dependence of the relaxation is related to the shape of the valence-band-tail distribution.

I. INTRODUCTION

Recent experiments have found that some of the localized states in a-Si:H are not permanently defined at the time of growth, but instead reach a glasslike thermal equilibrium in the temperature range 100–300 °C.[1,2] The equilibrium state in doped a-Si:H involves both dangling-bond defects and dopant states, and is observed as an increase in the doping efficiency with temperature.[2–4] The high-temperature state can be frozen in by quenching to room temperature, where the time constant for reequilibration is very long. In undoped a-Si:H, photothermal-deflection-spectroscopy (PDS), photoconductivity, and ESR experiments are reported to show that the equilibrium defect density increases with temperature, and, like the doped material, the higher defect densities can be frozen in by quenching.[1,5–7] However, some ESR experiments have found the opposite effect, namely that the defect density decreases with increasing temperature, and after quenching to room temperature the slow relaxation is seen as an increase in the defect density.[8] The explanation of the difference in the results has been unclear. This paper reports additional ESR data showing a neutral-defect density which increases with temperature.

The thermal equilibrium defect density N_D is given by an expression of the form

$$N_D = N_0 \exp(-U/kT) , \tag{1}$$

where U is the defect-formation energy and N_0 is a density of states. Thus, N_D should increase with temperature when the formation energy is positive. A simple model would suggest that N_0 is of order the silicon (or perhaps hydrogen) atom density in the material. The observed defect density of about 10^{15} cm^{-3} then requires a large value of U and so a strong temperature dependence. The previous measurements, however, report that the actual temperature dependence of N_D is quite weak. Smith and Wagner were able to reconcile the theory and experiment by introducing a distribution of formation energies.[9] They argued that most of the defects originate from a small fraction of weak-bond sites where the formation energy is small. In their model, they associated the distribution of formation energies with the shape of the valence-band tail. Here we argue that the predicted defect density also depends on the specific microscopic defect reaction. Some specific defect-formation models are analyzed in some detail and the results compared with experiment.

Another characteristic property of the equilibrium is the time required for structural relaxation, which has been found to be thermally activated,[5]

$$\tau = \tau_0 \exp(E_B/kT) , \tag{2}$$

where τ_0 is a prefactor of order 10^{-10}–10^{-12} sec, and E_B is an energy barrier for structural rearrangements. The activation energy has been associated with the diffusion barrier of hydrogen, and a quantitative link was made between the dispersive hydrogen diffusion and the stretched exponential equilibration of the electronic states.[10] According to this model, the equilibration is expected to be slower in undoped a-Si:H than in doped material, because the hydrogen diffusion coefficient is lower.[11] We report measurements of the relaxation rates which confirm this prediction, with results that are consistent with the stretched exponential kinetics. The annealing of light-

induced defects follows similar relaxation kinetics, although the time constants are not exactly the same. A possible explanation for the difference is discussed.

II. EXPERIMENTAL RESULTS

The ESR measurements were made on undoped plasma deposited *a*-Si:H films. Thick samples were grown (20–90 μm), so that the bulk defect states would dominate over any surface states and would also be easy to detect by ESR. The samples had thin p^+- and n^+-type contact layers which further suppresses any possible surface ESR signal. The samples were deposited on glass substrates held at 230 °C. In some cases the glass was coated with a very thin film of chromium to help adhesion. The samples were deposited with the normal deposition conditions, except that the rf plasma power was larger than is usually used to make low-defect-density material. Samples were grown at rf power from 10 to 50 W instead of the usual 2 W. The higher power raised the growth rate and so allowed thick films to be deposited in a reasonable time (up to 2 days). The higher power also raised the defect density slightly to the range 3×10^{15}–3×10^{16} cm^{-3}. The spin density varied from run to run by about a factor of 3, which is not unusual for *a*-Si:H films. The origin of the variation is undetermined, but may be caused by uncontrolled variations in the growth conditions during these very long runs. In particular, the reactor pressure tended to vary during the depositions. All the samples investigated exhibited the same general equilibration effects. The most detailed relaxation data were measured on one 40-μm sample with a spin density of about 10^{16} cm^{-3}, but all the other samples had a similar form of relaxation. Data for the equilibrium defect density are given for samples of different thickness and spin density.

In most measurements, the sample was first annealed at 290 °C for 10 min and then rapidly cooled to room temperature for ESR measurements. The samples were then annealed at intermediate temperatures of 180–250 °C for increasing time periods, again measuring the spin density at room temperature after each anneal step. The ESR signal was the $g=2.0055$ resonance attributed to neutral dangling bonds. The initial anneal establishes the equilibrium defect density at high temperature, and the subsequent anneals define the time-dependent relaxation to the new lower-temperature equilibrium. The relaxation data are used to determine when the equilibrium state is reached, and also to confirm that the quenching rate is fast enough to freeze in the structure at the anneal temperature. Subsequent anneals to the initial temperature were performed to confirm that the changes were reversible. In some cases the complete annealing curves were not measured and instead the necessary annealing time to reach equilibrium was inferred from relaxation data at other temperatures.

The relaxation data for a 40-μm, 10-W sample are shown in Fig. 1. The equilibration takes about 3×10^5 sec to complete at 200 °C, decreasing by 2 orders of magnitude at 250° C. The time dependence is nonexponential and is consistent with the stretched exponential form found in doped material,[10]

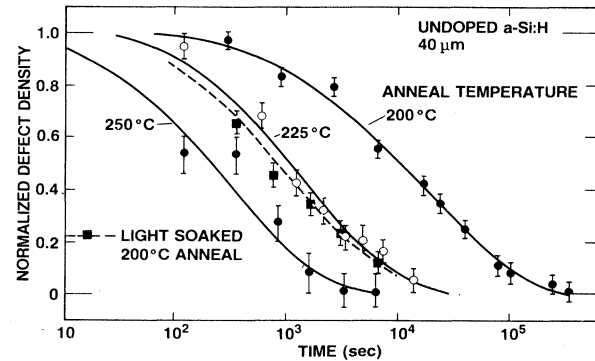

FIG. 1. Relaxation data at different temperatures for a 40-μm (10 W rf) sample after quenching from 290 °C. Also shown is the relaxation at 200 °C after prolonged room-temperature light soaking.

$$\Delta N=\Delta N_0 \exp[-(t/\tau)^{\beta}] \ . \tag{3}$$

The dispersion parameter β is 0.6 ± 0.05 at 200 °C, and seems to increase with temperature, as is observed in doped *a*-Si:H. However, the experimental uncertainty in the ESR spin density, and the limited temperature range of the measurements, do not allow an accurate evaluation of the temperature dependence of β.

The relaxation data in Fig. 1 are normalized to the initial and final ESR spin densities. In each series of measurements the initial density was the same within experimental uncertainty, showing that the equilibration is indeed a reversible effect. The steady-state spin densities at the various equilibration temperatures are shown in Fig. 2. The equilibrium defect density increases by about a factor of 2 between 200 and 300 °C. Data are also shown in the figure for several other samples. The 90-μm sample had a similar absolute spin density and equilibrium properties, and the 45-μm sample had a lower spin density. Both samples were deposited under the same nominal deposition conditions as the 40-μm sample with 10 W rf power. Data are also shown for a 20-μm sample deposited at 30 W and a 50-μm sample at 50 W, both of which had higher defect densities than the 10-W samples. In each case the temperature dependence of N_D is similar, with an activation energy of about 0.18 eV and a prefactor, defined by Eq. (1), of roughly $(1-5)\times10^{17}$ cm^{-3}. The 20-μm sample was annealed up to 400 °C, and was quenched in cold water above 300 °C to increase the cooling rate and ensure that the equilibration temperature was equal to the anneal temperature. No irreversible changes were found even at this high temperature, and the total range of the defect density was about a factor 4. Irreversible changes due to hydrogen evolution would presumably be seen at sufficiently high anneal temperatures and long anneal times.

Our results confirm that the equilibrium ESR spin density increases with temperature, and they are qualitatively similar to the results reported in Refs. 1 and 5–7, but are in contrast with the opposite behavior reported by Lee *et al.*[8] Xu *et al.* have reported evidence that those observations may be influenced by surface states.[7]

The temperature dependence of the relaxation-time constant is shown for two samples in Fig. 3, and is compared with the photoconductivity equilibration data of McMahon and Tsu,[5] and also with the results of sweep-out data on n-type a-Si:H.[4] The time constants are thermally activated with an energy of about 1.5 eV and are substantially larger than in the doped material. The values for the two samples differ by a factor of 4, with the sample with the lowest defect density having the smallest time constants. Our values of τ are also considerably larger than those found by McMahon and Tsu at the same temperatures, even though both measurements are on undoped material. The sample they used was deposited in our reactor with a rf power of 2 W. Some caution is needed in the comparison with their results because the experimental techniques are different. However, the agreement in the relaxation times for light-induced defects measured by the two methods, as described shortly, is evidence that the comparison is valid.

It is evident that the relaxation times depend on the sample-deposition conditions. Figure 4 shows that the relaxation time at a fixed temperature of 225 °C increases

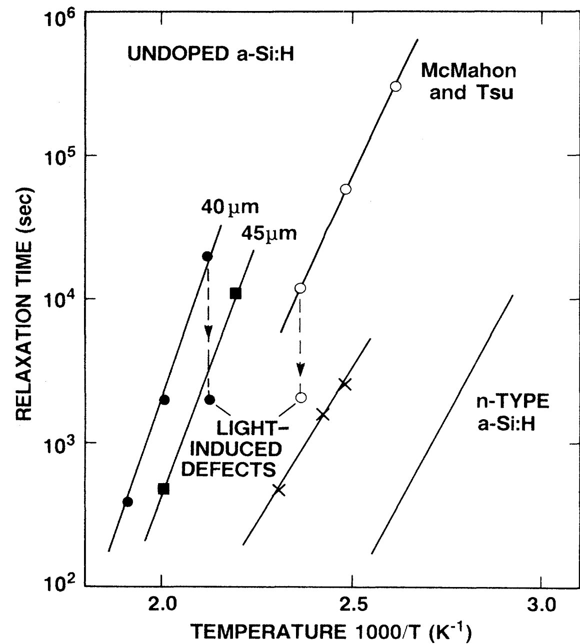

FIG. 3. Temperature dependence of the relaxation times taken from relaxation data as shown in Fig. 1. Data for two samples are shown as are effects of light soaking. Also plotted are equilibration data taken from Ref. 5 (open circles), light-soaking data from Ref. 13 (crosses), and thermal equilibration data of n-type a-Si:H from Ref. 3 (solid line).

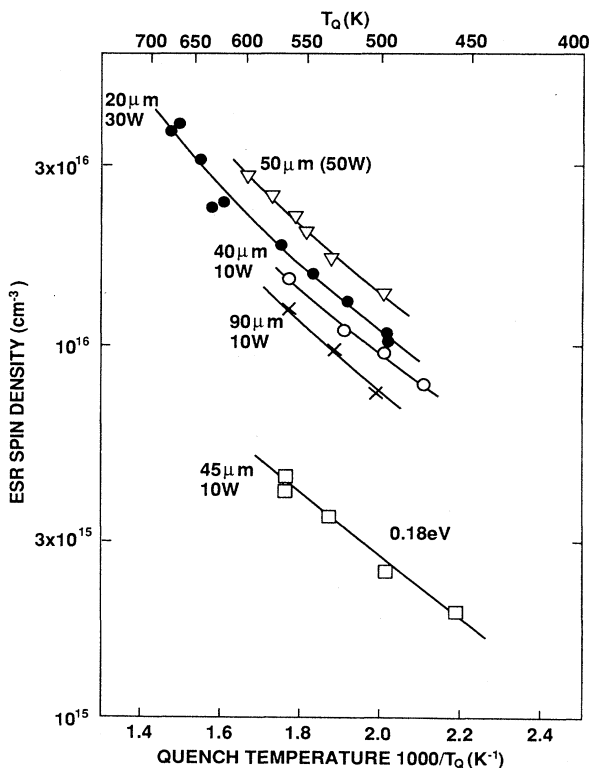

FIG. 2. Dependence of the equilibrium spin density on quench temperature for five samples. The thicknesses of the samples and rf power during deposition are shown.

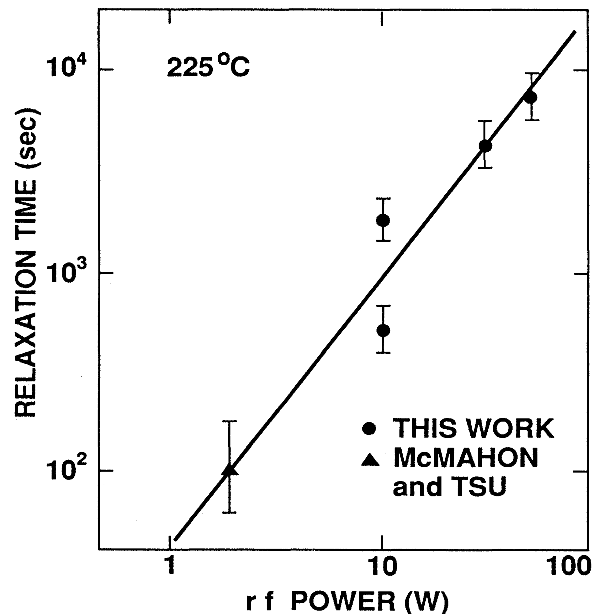

FIG. 4. Dependence of the relaxation time at 255 °C on rf power during deposition, including data from Ref. 5.

with rf power by nearly 2 orders of magnitude over the range investigated. Previous studies have found that the time constant also increases with rf power in n-type samples.[12] The origin of the different relaxation rates is presumed to be a different hydrogen diffusion coefficient caused by some modification of the structure, but as yet we have no direct evidence. The defect density also increases with rf power, so that this quantity is also correlated with the relaxation time. A possible explanation of the link between the spin density and the relaxation time is discussed further in Sec. IV B.

McMahon and Tsu also reported that the light-induced defects anneal faster than thermally induced defects by about an order of magnitude.[5] This result is particularly interesting because of the supposition that both relaxation processes correspond to the reequilibration of the structure. Data inferred from their paper are shown in Fig. 3, and agree quite well with earlier ESR measurements of the relaxation times of light-induced defects,[13] which are also shown in the figure. We have made the same comparison with the 40-μm sample and also observe the effect. In this measurement the sample was first allowed to equilibrate at 200 °C, and then was illuminated at room temperature with filtered white light. The illumination time of several hours was chosen to cause the spin density to roughly double, which is the same change that results from an anneal at 290 °C. The relaxation was then measured at 200 °C, using the same method as for the annealing experiments. The decay data are shown in Figs. 1 and 3, and are indeed found to be about an order of magnitude faster than for the thermally annealed sample. The actual magnitude of the relaxation times for both the light-induced and thermal defects are different from that found by McMahon and Tsu. The result suggests that the two time constants are related, and that the different deposition conditions cause both to increase proportionally. McMahon and Tsu interpret the different time constants as indicating that the higher temperature of thermal defect creation creates more stable defects than with optical illumination. This point is discussed further in Section IV B.

III. THERMODYNAMIC EQUILIBRIUM MODELS

There seems to be little doubt that the temperature dependence of the defect density is due to defect equilibration. The thermodynamic equilibration density can be calculated from a specific defect-formation model, provided the formation energy is known. There have been several calculations of the equilibrium defect density for both doped and undoped a-Si:H.[5,9,14–16] Here we adopt the same approach as used by Smith and Wagner,[9] and to varying degrees by several other groups, and make three key assumptions.

(1) There is a nonequilibrium distribution of strained silicon-silicon bonds which originates from the disorder of the a-Si:H network and which varies with deposition condition and sample treatment. The distribution is nonequilibrium in the sense that the strain energies do *not* have a temperature-dependent Boltzmann distribution.

(2) Defects are caused by the breaking of weak Si—Si bonds, with which they are in thermal equilibrium, in the sense that the defect density is given by the minimum free energy of the ensemble of weak bonds and defects. The nonequilibrium distribution of weak silicon bonds implies that there will be a distribution of defect-formation energies, because the energy depends on the specific bond that is broken.

(3) The defect-formation energy U is equated to the difference in one-electron energies of the defect gap state at E_D, and the valence-band-tail state from which it is derived. Thus,

$$U = E_D - E_{\rm VB} \ , \tag{4}$$

where $E_{\rm VB}$ is the energy of a state in the valence-band tail. This is the weak-bond–dangling-bond conversion model described by Stutzmann.[17] Equation (4) is an approximation to the difference in total energy, and neglects ionic and relaxational energies. Certainly the electronic energies are an important contribution to the formation energy, but it has not yet been proved that the other terms in the total energy of the states are really negligible. Nevertheless, it seems to be quite a good approximation.[18]

The defect creation is described by the general reaction

$$\textit{weak bonds} \leftrightarrows \textit{defects} \ . \tag{5}$$

However, this is insufficient to completely specify the thermodynamics, and various alternative models can be considered. We analyze four specific reactions to illustrate the possibilities, but there may be other reactions.

It is essential to include in the calculations the distribution of formation energies, which originates from the variation of strain energies of the silicon bonds. According to the weak-bond model, the distribution function is equated to the shape of the valence-band tail, which we assume to be an exponential of the form

$$N_v(E_{\rm VB}) = N_{v0}\exp(-E_{\rm VB}/kT_V) \ . \tag{6}$$

We define the valence-band distribution as the density of eigenstates, each of which can be occupied by two electrons, rather than the total density of electrons. The parameters of the model will be described shortly. The formation energy as defined by Eq. (4) contains the defect-gap-state energy, which will also be distributed in energy. The initial calculations are performed neglecting this distribution, and then we show how it modifies the results.

Thermodynamic calculations can be performed either by minimizing the free energy or by applying the law of mass action to the defect reactions, with identical results. The identity is shown explicitly for the first case, and thereafter the mass-action expressions are used.

A. Model 1

The first model to be considered seems the most obvious and is the conversion of one weak bond into one neutral singly occupied dangling bond. Only silicon atoms are considered. The free energy of N_D defects and $N_0 - N_D$ weak bonds, where N_0 is the total density of

possible sites of formation energy U, is

$$F(N_D)=N_D U-kT\ln\left[\frac{N_0!}{N_D!(N_0-N_D)!}\right]$$
$$\simeq N_D U-kT\left[N_0\ln\left[\frac{N_0}{N_0-N_D}\right]-N_D\ln\left[\frac{N_D}{N_0-N_D}\right]\right] . \quad (7)$$

This expression assumes a lattice-gas model and implicitly excludes any contribution to the entropy from changes in the phonons, etc. Minimizing the free energy with respect to N_D leads to the following expression for the equilibrium defect density,

$$N_D(T)=\frac{N_0 e^{-U/kT}}{1+e^{-U/kT}} , \quad (8)$$

which is a standard derivation, often used to obtain the equilibrium concentration of defects in a crystal.

Application of the law of mass action to reaction (5) gives

$$N_D=N_{\mathrm{WB}}\exp(-U/kT) , \quad (9)$$

It is important to note that the prefactor on the right-hand side is the density of unconverted weak bonds (N_0-N_D) rather than N_0. Equation (8) immediately follows when this substitution is made.

The distribution of formation energies is accounted for by integration of N_D in Eq. (8) over the distribution of U, given by Eqs. (4) and (6), to obtain

$$N_D\simeq\frac{N_{v0}kTT_v}{T_v-T}\left[\frac{T_v}{T}\exp(-E_D/kT_v)-\exp(-E_D/kT)\right] . \quad (10)$$

Virtually all the states for which $U<0$ convert into defects, and a temperature-dependent fraction of those with $U>0$ convert. The defect chemical potential can be equated with the energy E_D of the neutral defect, because there the formation energy is zero, and exactly half the weak bonds will have converted to defects.

So far, we have considered only defects with a single energy in the gap. However, neutral defects in undoped *a*-Si:H are known to be distributed in an approximately Gaussian band ~ 0.1 eV wide. Bar Yam *et al.*[16] first pointed out that the minimization of the free energy of the broadened defect band will cause a shift of the defect gap state energy level. We can reproduce this behavior and take into account phenomenologically the effects of site-dependent defect-formation energies by assuming a Gaussian distribution of defect chemical potentials. The resulting equilibrium concentration of neutral defect states is then given by an integral of the defect density over the distribution of defect-gap-state energies. For the model under consideration, this integral is

$$N_D(T)=\frac{N_{v0}kTT_v}{T_v-T}\int_0^\infty\left[\frac{T_v}{T}e^{-E/kT_v}-e^{-E/kT}\right]\times\frac{e^{-(E-E_\mu)^2/2\sigma^2}}{(2\pi\sigma^2)^{1/2}}dE , \quad (11)$$

where E_μ is the most probable defect chemical potential, σ is the Gaussian width, and the integral is over the defect energy levels. Integration gives

$$N_D(T)\simeq\frac{N_{v0}kTT_v}{T_v-T}\times\left[\frac{T_v}{T}e^{-E_D/kT_v}e^{-\sigma^2/2(kT_v)^2}-e^{-E_D/kT}e^{-\sigma^2/k^2TT_v}e^{\sigma^2/2(kT)^2}\right] , \quad (12)$$

where the approximation involves neglect of an error function in the second term in the large parentheses which deviates significantly from 1 only when $T\gg T_v$, and E_D is now defined by

$$E_D=E_\mu-\frac{\sigma^2}{kT_v} . \quad (13)$$

At low temperature the defect density is dominated by the first term in large parentheses in Eq. (12). To a good approximation, Eq. (12) is identical to the formula for a discrete gap state [Eq. (10)], except that the defect energy E_D is shifted from the average defect chemical potential E_μ by the energy σ^2/kT_v, and the effective density of valence-band-tail states is reduced by a factor $\exp[-\sigma^2/2(kT_v)^2]$. A similar result also applies to the other models discussed below. The experiments measure E_D rather than E_μ, so that the correction is taken care of automatically by using the experimental determined peak gap-state energy. Measured values of the defect bandwidth are imprecise, but lie in the range 0.2–0.3 eV, corresponding to $\sigma\approx 0.1$ eV. The predicted shift of the peak is therefore about 0.2 eV, when $kT_v\approx 45$ meV, and the effective density of band-tail states is reduced by about a factor of 10. Thus, a first-order correction of the expressions calculated for a discrete gap state, to account for the distribution, is obtained by using the experimentally measured position of E_D and reducing the effective density of valence-band-tail states. This is the approach used to evaluate the different models.

Values of the various parameters are needed to compare the theory with experiment. The density of states that we use is shown in Fig. 5. Time of flight, photoemission yield, and optical absorption give the valence-band-tail slope as 500 K.[19–21] The exponential slope continues up to a density of about 10^{21} cm^{-3}eV^{-1}, above which the band tail is more nearly linear. Our zero of energy is the top of the exponential tail, as defined in the figure, and we estimate this energy to be about 0.1 eV above the valence-band-mobility edge. The value of N_{v0} used in all our calculations is taken to be a factor of 5 less than the actual density of states, because of the effect of the distribution of the gap states just described, and so is set at

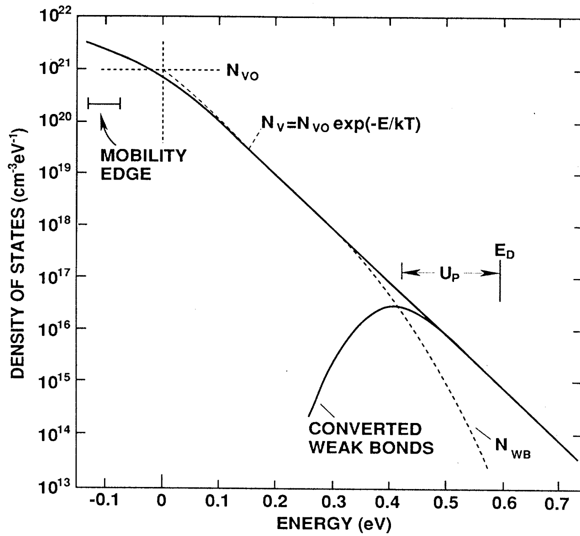

FIG. 5. Schematic density-of-states diagram, showing the measured valence-band-tail distribution N_v, and illustrating the conversion of weak-bond states $N_{\rm WB}$ into defects. E_D is the assumed gap-state energy of the defect, and the energy U_P is explained in the text. Note that the zero of energy is not the mobility edge.

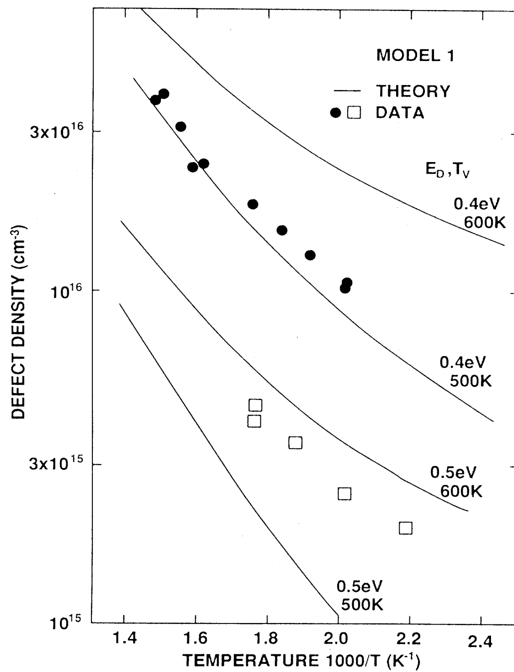

FIG. 6. Temperature dependence of the defect density for model 1 obtained from an evaluation of Eq. (10), for the parameters E_D and T_v shown. $N_{\rm H}$ taken to be 5×10^{21} cm^{-1}, and N_{v0} is 2×10^{20} cm^{-1}eV^{-1}, as discussed in the text. The data are taken from Fig. 2.

2×10^{20} cm^{-1}eV^{-1}. The concentration of Si—H bonds is equated to the total hydrogen concentration of about 5×10^{21} cm^{-3}. There is some disagreement over the location of the neutral defect energy levels in the gap. An energy of 0.6 eV (from our assumed zero of energy) is obtained by photoemission yield and is consistent with other measurements.[20]

Plots of the defect-density temperature dependence of model 1 [Eq. (10)] are shown in Fig. 6 and compared to some of the experimental data from Fig. 2. The curves illustrate a range of values of E_D and T_v. The temperature dependence and the correct overall magnitude of the data can be reproduced by the theory, at least for some set of parameters. However, the defect density is much too low when we use the experimental values, $E_D=0.6$ eV and $T_v=500$ K. The choice of parameters is discussed further in Sec. IV A.

When a weak bond is broken, two dangling bonds are created. A crucial assumption of model 1 is that the defects separate and move to isolated sites. The silicon lattice must be flexible so that one-half of the broken bond can reconstruct with another half of a broken weak bond elsewhere. Pantelides has argued that floating-bond defects have the capability to move by a bond-switching mechanism, which could allow the reconstruction.[22] However, the proposed floating-bond model is more complicated, involving the interconversion with dangling bonds and both types of defects in the equilibrium state. The thermodynamics have not yet been worked out, and will certainly depend on the detailed assumptions made.

Model 1 can only apply if the silicon defect states are mobile. There is, as yet, no clear experimental evidence for mobile defects, and other solutions to the problem of separating the defects are possible. For example, the two defects of a broken weak bond may remain localized at the same bond, and this situation is analyzed as Model 2. Alternatively, the motion of bonded hydrogen can cause the separation of the defects. In this case the entropy of the Si-H sites must be included in the calculations and this is done in models 3 and 4.

B. Model 2

The thermal equilibrium defect density will be different from that of model 1 if the defects do not diffuse apart. The conversion of a weak bond into a pair of defects which do not separate is governed by the reaction

$$\textit{weak bond} \rightleftharpoons (2D_0)_{\rm pair}\ . \tag{14}$$

The formation energy of the pair is $2U$, and following the same approach as for the previous model gives for the defect density,

$$N_D(T)=\frac{2Ne^{-2U/kT}}{1+e^{-2U/kT}}\ . \tag{15}$$

The factor 2 is included because there are two dangling bonds at each site. Integration over the distribution of formation energies gives

$$N_D(T) \simeq \frac{2N_{v0}kTT_v}{2T_v - T}\left[\frac{2T_v}{T}\exp(-E_D/kT_v) - \exp(-2E_D/kT)\right] . \quad (16)$$

This has the same general form as model 1, except that factors of 2 enter because the formation energy of the defect pair is $2U$. Both models 1 and 2 were considered by Smith and Wagner,[9,23] but our results differ from theirs in the number of available sites that is assumed, and in some aspects of the integration. The defect density is predicted to have a much weaker temperature dependence than in model 1. Some examples of the evaluation of Eq. (16) are given below.

In our opinion it is doubtful that this defect-reaction model can be correct because we expect no paramagnetic ESR signal when both defects remain localized at the same weak-bond site, even if relaxation allows the defects to move apart slightly. The ESR observations imply that the two defects created when a weak bond breaks must move apart. We next consider two models in which the motion of hydrogen is included as the specific mechanism of defect migration. Neither model has been analyzed in any detail before.

C. Model 3

A defect mechanism often suggested is that hydrogen is released from a Si—H bond and breaks a weak Si—Si bond, thus creating two defects by the reaction

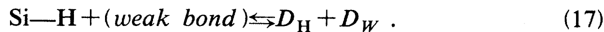

$$\text{Si—H} + (\textit{weak bond}) \leftrightarrows D_{\text{H}} + D_W . \quad (17)$$

The model is illustrated in Fig. 7. The defect labeled D_W refers to the one at the site of the weak bond, where it is immediately adjacent to the Si—H bond. This defect cannot be separated from the Si—H bond and the two

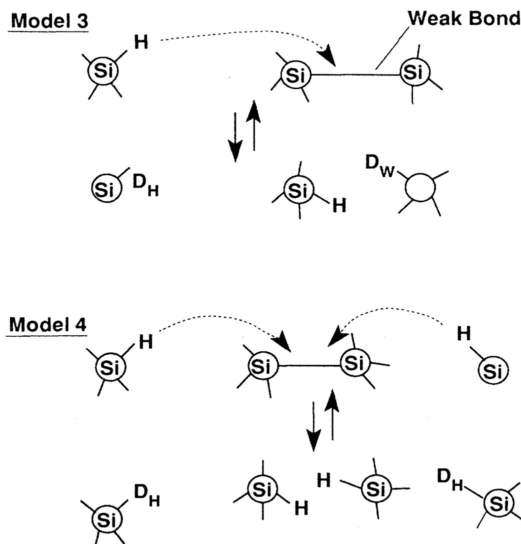

FIG. 7. Schematic illustrations of the defect reactions corresponding to models 3 and 4 analyzed in the text.

must be considered a single entity. The isolated D_{H} defect is left by the removal of hydrogen from the Si—H bond. Although these defects may have identical electronic properties, they must be treated separately in the thermodynamic calculation. By the construction of the model, the two defect types have the same density, N_D, and the total defect density is $2N_D$. The law of mass action applied to reaction (17) gives

$$N_{D\text{H}}N_{DW} = N_D^2 = N_{\text{WB}}N_{\text{H}}\exp(-2U/kT) , \quad (18)$$

where the N's are the densities of the different sites and U is the energy to convert one weak-bond electron to a defect, as given by Eq. (4). The factor $2U$ enters because the reaction converts two weak-bond electrons into two defects. There is also a law of conservation of states, which in the assumed model is written as

$$N_{\text{WB}} + N_{DW} = N_v . \quad (19)$$

Here, N_v is the distribution of valence-band-tail states that would be present if no states were converted to defects, whereas N_{WB} is the actual density of weak-bond states. Thus,

$$N_D^2 = (N_v - N_D)N_{\text{H}}\exp(-2U/kT) , \quad (20)$$

which is quadratic in N_D and clearly different from the results of either model 1 or 2 [see for example, Eq. (9)].

The distribution of defect-formation energies is again introduced by associating a different density of valence-band-tail states with each formation energy as defined by Eq. (4). Care is needed in the analysis because the two defect types are not the same, and the assumption of the model is that only the weak bonds have a distribution of energies. This implies that all the defects formed by the removal of hydrogen from Si—H are equivalent, but that the D_W defects depend on which weak bond is broken. Consider a small portion of the valence-band distribution, $\delta N_v(U)$, for which the defect-formation energy is U. The density of defects $\delta N_{DW}(U)$ created from these states is given by [see Eq. (20)]

$$N_{D\text{H}}\delta N_{DW}(U) = [\delta N_v(I) - \delta N_{DW}(U)]N_{\text{H}}\exp(-2U/kT) . \quad (21)$$

There is the added constraint that the total number of defects on weak bonds equals the density on Si—H sites, so that

$$\int dN_{DW}(U) = N_D . \quad (22)$$

It follows, therefore, that N_D is the solution to the integral equation

$$N_D = \int \frac{N_{\text{H}}N_v(E)dE\,\exp(-2U/kT)}{N_D + N_{\text{H}}\exp(-2U/kT)} , \quad (23)$$

where the integral is over the distribution of tail states. Substituting for Eq. (6) gives

$$N_D = N_H N_{v0} \exp(-E_D/kT_v) \int \frac{\exp(U/kT_v)dU}{N_H + N_D \exp(2U/kT)} . \quad (24)$$

The result can be understood by looking at the limiting cases when U is either larger or smaller than U_p, where

$$U_P = (kT/2)\ln(N_H/N_D) . \quad (25)$$

The integral can be approximated as

$$N_D = \int_{U<U_P} N_{v0} \exp[(U-E_D)/kT_v]dU + \int_{U>U_P} \{N_H N_{v0} \exp[(U-E_D)/kT]\}^{1/2} \exp(-U/kT)dU . \quad (26)$$

The first term is the number of valence-band-tail states above $E_D - U_p$, and for these small formation energies virtually all the tail states are converted into defects. The second term is the contribution from weak bonds with energies larger than U_p, and the square root comes from the solution to Eq. (20) when $N_D \ll N_v$. The distribution of weak bonds that convert into defects and the remaining N_{WB} are illustrated in Fig. 5. Integration of Eq. (26) gives, for the total defect density,

$$2N_D(T) = \frac{2N_{v0}kTT_v}{2T_v - T} \left[\frac{2T_v}{T} \exp\left[-\frac{E_D + \frac{1}{2}kT\ln(N_D/N_H)}{kT_v} \right] - \exp\left[-\frac{2E_D + kT\ln(N_D/N_H)}{kT} \right] \right] , \quad (27)$$

which has a similar form as for models 1 and 2, except that N_D appears on the right-hand side.

An approximate explicit solution for the defect density is obtained by noting that the integrand of Eq. (24) peaks near U_P, and so we can write, for the total defect density,

$$2N_D \simeq 2kT_v N_v(U_P) = 2[kT_v N_{v0} \exp(-E_D/kT_v)]^{2T_v/(T+2T_v)} (N_H)^{T/(T+2T_v)} . \quad (28)$$

A numerical integration of Eq. (24) is shown in Fig. 8 and compared to the ESR data. A good fit is obtained when T_v is 500–600 K and $E_D = 0.6$–0.8 eV. The fit is similar to that of model 1 shown in Fig. 6, but the parameters are different, and in this case are in better agreement with the experimental data. Model 3 gives a larger defect density than model 1, so that the fit requires a steeper slope of the band tail and/or deeper defect-gap-state energy. The reason for the larger defect density is the extra entropy provided by the Si—H bonds, whose density is much larger than that of the weak-bond states (at least those for which the formation energy is low). The extra entropy is contained in the $\ln(N_H/N_D)$ term in the energy U_P, by which the defect chemical potential is shifted towards the valence-band edge from E_D. Since N_H/N_D is typically 10^6, $U_P \approx 6kT$.

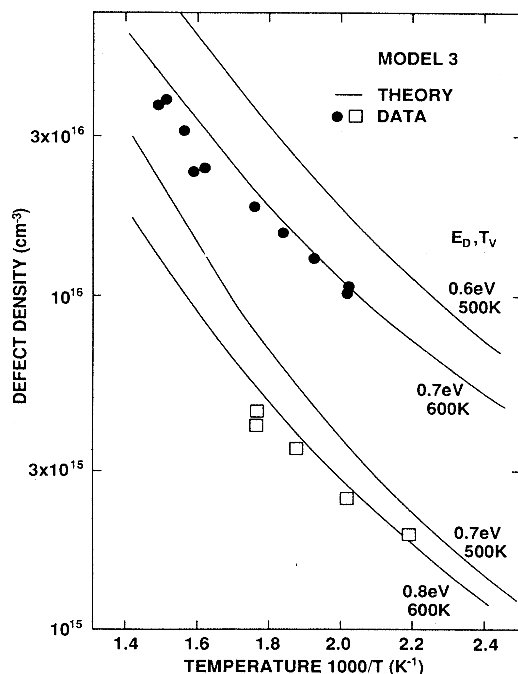

FIG. 8. Temperature dependence of the defect density for model 3 obtained from an evaluation of Eq. (24), for the parameters E_D and T_v shown. N_H is taken to be 5×10^{21} cm^{-1}, and N_{v0} is 2×10^{20} cm^{-1} eV^{-1}, as discussed in the text. The data are taken from Fig. 2.

D. Model 4

In the model just discussed, the weak bond creates two defects, one of which is constrained to remain in a singly hydrogenated weak bond and the other on an isolated *a*-Si—H bond from which the hydrogen is removed. Another reaction could be added in which a second hydrogen transfers from a Si—H state into the weak-bond defect, so that the two types of defect sites are allowed to interconvert,

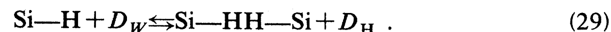

$$\text{Si—H} + D_W \leftrightarrows \text{Si—HH—Si} + D_H . \quad (29)$$

A simple model to explore is the case when the isolated D_H defect sites dominate over those remaining at weak bonds (see Fig. 7). All the weak-bond sites are then occupied by either zero or two hydrogen atoms. Combining reactions (17) and (29) and applying the law of mass action gives

$$N_D^2 = (N_{WB} N_H^2 / N_{WB\,HH}) \exp(-2U/kT) , \quad (30)$$

where $N_{WB\,HH}$ denotes the density of fully hydrogenated weak bonds. The difference between this expression and the mass-action formula of model 3 [Eq. (20)] again illustrates that the predicted defect density is sensitive to the details of the reaction. Following the same procedure as

before to include the distribution of formation energies, it can be shown that the defect density is the solution to

$$N_D=2N_H^2N_{v0}\exp(-E_D/kT_v)\int\frac{\exp(U/kT_v)dU}{N_H^2+N_D^2\exp(2U/kT)} . \tag{31}$$

The distribution of converted weak bonds has a peak below E_D; in this case shifted from E_D by an energy $U_P=kT\ln(N_H/N_D)$, which is twice the value in model 3. The same approximations as for model 3 gives, for the total defect density,

$$N_D\simeq 2kT_vN_v(U_P)=2[kT_vN_{v0}\exp(-E_D/kT_v]^{T_v/(T+T_v)}(N_H)^{T/(T+T_v)} . \tag{32}$$

The results of a numerical integration of Eq. (31) are shown in Fig. 9 for various E_D and T_v. The fit is not as good as for model 3 because the predicted temperature dependence is too large. Again, it is necessary to use different parameters to fit the data. The predicted defect density is higher than for model 3 because of the extra entropy gained by having both defects on isolated Si—H sites.

E. Summary

The four models can be summarized by the following equations. Each has a similar form, and includes the Gaussian broadening of the defect gap state.

Model 1:

$$N_{D_0}(T)\approx\frac{N_{v0}kTT_v}{T_v-T}\left[\frac{T_v}{T}\exp\left[-\frac{E_D}{kT_v}-\frac{\sigma^2}{2(kT_v)^2}\right]-\exp\left[-\frac{E_D}{kT_v}-\frac{\sigma^2}{k^2TT_v}+\frac{\sigma^2}{2k^2T^2}\right]\right] , \tag{33}$$

where $E_D=E_\mu-\sigma^2/kT$ is the peak of the observed band of neutral defect gap states.

Model 2:

$$N_{D_0}(T)\approx\frac{2N_{v0}kTT_v}{2T_v-T}\left[\frac{2T_v}{T}\exp\left[-\frac{E_D}{kT_v}-\frac{\sigma^2}{2(kT_v)^2}\right]-\exp\left[-\frac{2E_D}{kT}-\frac{2\sigma^2}{k^2TT_v}+\frac{2\sigma^2}{k^2T^2}\right]\right] . \tag{34}$$

This is obtained from model 1 by the transformation $T\to T/2$.

Model 3:

$$N_{D_0}(T)\approx\frac{2N_{v0}kTT_v}{2T_v-T}\left\{\frac{2T_v}{T}\exp\left[-\frac{E_D}{kT_v}-\frac{T}{2T_v}\ln\left[\frac{N_D}{N_H}\right]-\frac{\sigma^2}{2(kT_v)^2}\right]\right.$$
$$\left.-\exp\left[-\frac{2E_D}{kT}-\ln\left[\frac{N_D}{N_H}\right]-\frac{2\sigma^2}{k^2TT_v}+\frac{2\sigma^2}{k^2T^2}\right]\right\} . \tag{35}$$

This is the same as model 2 with the transformation $E_D\to E_D+\frac{1}{2}kT\ln(N_D/N_H)$.

Model 4:

$$N_{D_0}(T)\approx\frac{2N_{v0}kTT_v}{2T_v-T}\left\{\frac{2T_v}{T}\exp\left[-\frac{E_D}{kT_v}-\frac{T}{T_v}\ln\left[\frac{N_D}{N_H}\right]-\frac{\sigma^2}{2(kT_v)^2}\right]\right.$$
$$\left.-\exp\left[-\frac{2E_D}{kT}-2\ln\left[\frac{N_D}{N_H}\right]-\frac{2\sigma^2}{k^2TT_v}+\frac{2\sigma^2}{k^2T^2}\right]\right\} . \tag{36}$$

This is the same as model 2 with the transformation $E_D\to E_D+kT\ln(N_D/N_H)$.

IV. DISCUSSION

Our experimental results add to the mounting evidence that defects in *a*-Si:H are in thermal equilibrium.[1–8,24] The characteristic signature of the equilibrium is a reversible temperature-dependent change in the defect density, and a thermally activated relaxation time. Most reported measurements have been performed on films prepared by glow discharge at the optimum growth conditions. Our results show that equilibration also occurs in samples deposited at high rf power, and others have observed the effect in sputtered material.[24] There is, however, no direct confirmation yet of equilibration in samples made at more extreme deposition conditions; for example, very different deposition temperatures.

It is well known that the defect density of samples de-

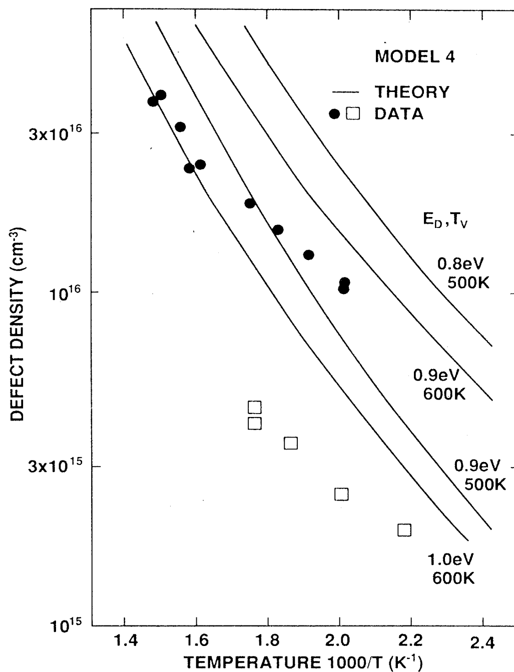

FIG. 9. Temperature dependence of the defect density for model 4 obtained from an evaluation of Eq. (31), for the parameters E_D and T_v shown. N_H is taken to be 5×10^{21} cm^{-1}, and N_{v0} is 2×10^{20} cm^{-1} eV^{-1}, as discussed in the text. The data are taken from Fig. 2.

posited below 150 °C decreases irreversibly when the sample is annealed to 200–300 °C, and increases again at higher anneal temperatures due to hydrogen evolution. It is important to note that these irreversible changes in defect density do not preclude the equilibrium model. The thermal equilibrium interpretation of these results is that annealing causes an irreversible change in the silicon bonding structure. The resulting change in the distribution of weak bonds (and hence valence-band-tail states) then causes the defects to attain a different equilibrium density. Some evidence to support this view is described in the next subsection. We believe that equilibration probably occurs over the complete range of deposition conditions, including substrate temperature, as was proposed by Smith and Wagner.[9]

A. The equilibrium defect densities

The different thermodynamic models have some common features, even though they predict different defect densities. All predict a weak temperature dependence of the defect density, the origin of which is the distribution of formation energies, which provides sites with a low formation energy. At the limit of low temperature, $T\rightarrow0$, all the models reduce to the same result,

$$N_D(0)=2kT_vN_{v0}\exp(-E_D/kT_v)\ , \tag{37}$$

which is just the number of valence-band-tail states above E_D. The factor 2 originates from our definition of N_v in Eq. (6) as the density of eigenstates rather than of electrons, and is replaced by a factor of unity in model 1 because of the assumed reconstruction of the bonds. The general result is that at low temperatures all weak-bond–dangling-bond conversion models tend to the same limit, and that the differences in the microscopic mechanisms are only significant at high temperatures. The reason that the models converge to the same limit is because the differences in entropy in the free energy (U-TS) becomes unimportant as $T\rightarrow0$. The four models have the same formation energies, but differ in the entropy factors.

Figures 10 and 11 compare the calculated temperature dependence of N_D for the four models, using the same parameters for E_D, T_v, and the density of states. The two figures show results for assumed values of T_v of 500 and 900 K. The curves in Fig. 10 diverge as the temperature is raised, with model 2 having the lowest defect density and model 4 the highest. The difference in defect density of more than 3 orders of magnitude reflects the different entropy terms. Model 4 allows the defects to move among a large density of Si—H sites, whereas the defects are confined to a much smaller density of weak bonds in models 1 and 2. One of the models analyzed by Smith and Wagner allowed the defects to reside at all the silicon sites, but this seems to conflict with the assumptions of the model.[9,23] Figure 11 shows that the difference in the predicted defect densities for the four models is greatly reduced when the band-tail slope T_v is increased. In the limit of large T_v, the results for all the models tend to the low-temperature limit given by Eq. (37).

In principle, the magnitude and temperature depen-

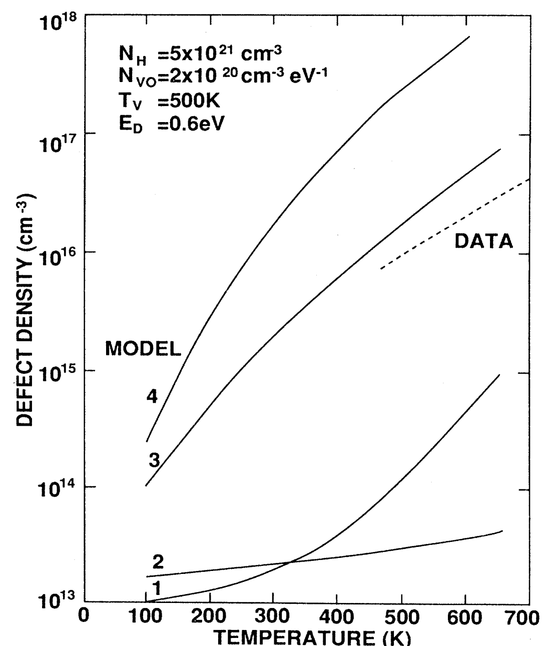

FIG. 10. Comparison of the temperature dependence of the defect density for the four different models. The band-tail slope is 500 K and the other parameters are indicated in the figure.

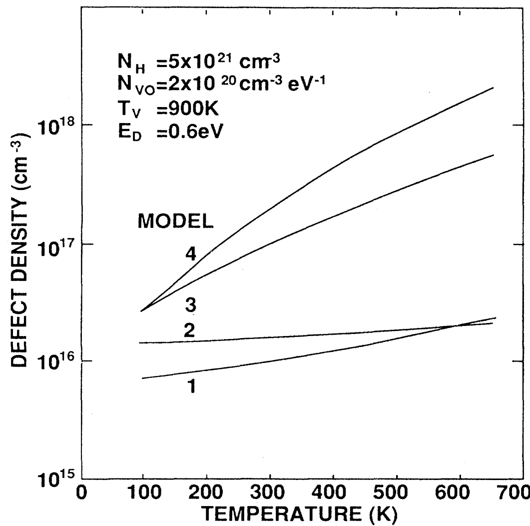

FIG. 11. Comparison of the temperature dependence of the defect density for the four different models. The band-tail slope is 900 K and the other parameters are indicated in the figure.

dence of the measured defect density could distinguish between the different reactions. However, there is still much that is left out of the analysis. We have not considered that the Si—H bond energies may vary from site to site, nor do we know whether all the bonded hydrogen is available to form defects. The formation energy given by Eq. (4) is an approximation, and any correction term will modify the calculated defect density. Nevertheless, our analysis finds that all weak-bond–dangling-bond conversion models predict the low activation energy of N_D as observed. We conclude that it is essential to include the distribution of formation energies in the analysis, and that the basic assumptions of the weak-bond–dangling-bond model appear to be valid.

There are some physical constraints on the different models. Model 1 requires the diffusion of silicon defects, whereas in models 3 and 4 it is the hydrogen that moves. In model 2 the defects do not diffuse apart. An experimental test of model 1 would be to observe equilibration or defect motion in unhydrogenated *a*-Si:H, but as yet no such effects have been reported. The fit to model 1 requires a defect energy level which is substantially shallower than that found by experiment. Model 2 requires paired defects, which is not consistent with the ESR data, and so we believe that this model can be discarded.

The presence of hydrogen provides a mechanism to separate the defects. Furthermore, the relaxation rate is accounted for by the known diffusion rate of hydrogen in *a*-Si:H.[25,26] Of the two hydrogen-related models analyzed, model 3 gives the better fit to the data, with valence-band and defect parameters that are close to those found by other measurements. Model 4 predicts a more rapid temperature dependence than is observed, and also requires a defect energy level that is further into the gap.

The distribution of valence-band-tail and defect states is quite accurately known for undoped *a*-Si:H films deposited under low-rf-power conditions.[19–21] The uncertainty in T_v is no more than 30 K in these films, while that in E_D is about 0.1 eV. There is less information about the density-of-states distribution of higher-rf-power samples, and so the uncertainty in the parameters is correspondingly larger. Therefore, we conclude that the temperature dependence and magnitude of N_D is best accounted for by model 3, but we cannot conclusively rule out model 4 because of the uncertainties of the formation energy in the weak-bond model and the appropriate parameters for our films.

Smith and Wagner pointed out that the equilibrium model predicts a relation between the defect density and the band-tail width.[9] Equations (28) [or (24)] and (32) [or (31)] define the relation for the two hydrogen-related models, and Eq. (37) describes the relation at low temperature for all the models. Figure 12 shows the dependence of N_D on band-tail slope for model 3, obtained by numerical integration of Eq. (24), for a range of equilibration temperatures. The predicted defect density increases rapidly with T_v, but is not a strong function of the equilibration temperature, because N_D is only weakly temperature dependent. The relation between N_D and T_v varies between the different thermodynamic models, but the general trend is the same. Experimental data lie between the 400- and 600-K lines,[27,28] which is the measured range of equilibration temperatures. The predicted dependence on T_v is obeyed quite well over a wide range of sample conditions, giving support to the model that equilibrium between defects and localized tail states determines the defect density under all deposition conditions.[9]

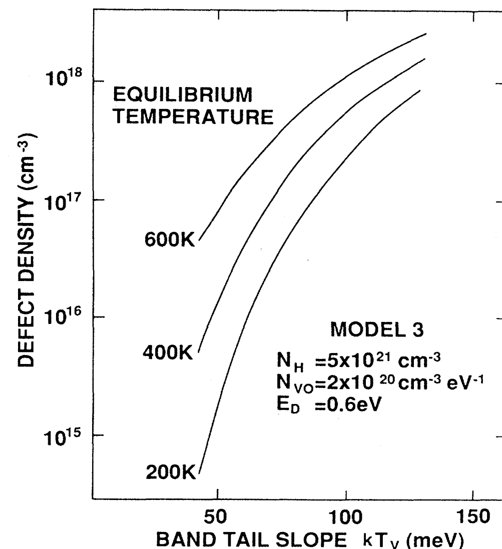

FIG. 12. Plot of predicted defect density vs band-tail slope at different equilibration temperatures, for model 3, obtained by numerical integration of Eq. (24).

B. The kinetics of thermal and light-induced defects

The time dependence of the spin-density relaxation in Fig. 1 measures the kinetics of the structural changes which enable the annealing of defects. For model 1 this would be a measure of the rate of silicon defect diffusion, which must then have an activation energy of 1.5 eV. For models 3 and 4 the time constant is associated with the diffusion of hydrogen, which is known to have an energy of 1.5 eV.[11] The evidence that hydrogen motion is the rate-limiting process is discussed in our previous studies of the equilibration kinetics in doped *a*-Si:H.[3,4,10] There has also been a detailed analysis showing a quantitative connection between the relaxation time of the thermal equilibration and the diffusion rate of hydrogen.[26]

At first consideration, there is no obvious connection between the hydrogen diffusion rate and the defect-formation energies, since the former depends on the Si—H bond strengths, and the latter on the band-tail and defect energies. However, the models for defect creation suggest that there is such a relation. In the reaction of Eq. (17) for model 3, the formation energy is obtained from the one-electron energy levels of the valence-band tail and the defects. The formation energy can also be stated in terms of the hydrogen binding energies. Referring to Fig. 7(a), two defects are created when hydrogen is released from a Si—H bond and is subsequently trapped at the weak bond. The defect-formation energy for the pair is therefore the difference in the hydrogen binding energies for these two configurations.

We therefore propose the simple description of the hydrogen bonding illustrated in Fig. 13. This figure schematically plots the energy of hydrogen in three different site types, and is intended to represent the physical mechanism of model 3. The hydrogen energy along the horizontal axis refers to the binding energy of the hydrogen at the particular bonding site. The Si—H bonds are the lowest-energy configurations (i.e., most strongly bound) and lie below the hydrogen chemical potential, μ_H. The Si—Si bonds lie at higher hydrogen energy and are mostly unoccupied by hydrogen, although hydrogen can break the weakest bonds. The D_H and D_W defects created by hydrogen trapping at these weak bonds have the distribution shown, and in equilibrium tend to cluster around μ_H. Note that the different hydrogen binding energies of the two defects are not in conflict with their having identical gap-state energies. Our model assumes that hydrogen can also be thermally excited into the mobile interstitial sites shown in the figure. Hydrogen diffusion data indicate that the interstitial level is about 1.5 eV about the Si—H bonds.

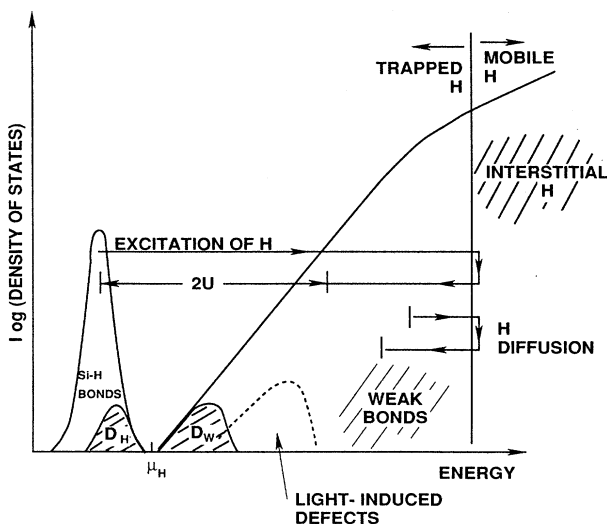

FIG. 13. Schematic diagram of the distribution of hydrogen binding energies, showing the Si—H bonds, the weak bonds, and hydrogen interstitial states. The figure is explained in the text.

The motion of hydrogen occurs by the excitation of a hydrogen atom from Si—H to the mobile states, followed by trapping into a weak bond. This is the very process described by model 3. The excitation of the hydrogen into the weak bond requires a net energy $2U$, which is $2E_D-2E_{VB}$ in the weak-bond model, and the concentration of hydrogen trapping sites is equal to the weak-bond density. There is, therefore, a mapping of the hydrogen binding energies onto the defect-formation energies. Within the approximations of this approach, the distributions of valence-band-tail states, defect-formation energies, and hydrogen binding energies have the same origin. According to this model, the concentration of hydrogen trapping sites at energy E above the hydrogen chemical potential is equal to the density of weak bonds with energy $E/2$ above E_D. Thus the hydrogen distribution is given by

$$G_H(E) \sim N_{WB}(E/2) \sim \exp(-E/2kT_v) . \quad (38)$$

Well above the chemical potential, the distribution of weak-bond energies, N_{WB}, equals the band-tail density of states N_v. The distribution of hydrogen bonding energies in Si—Si bonds therefore has the same shape as the valence-band tail, except for the doubling of the energy scale, and so will be an exponential of slope $2T_v$. The stretched exponential relaxation during equilibration has been interpreted in terms of the dispersive diffusion of hydrogen in an exponential distribution of trapping sites.[10] The parameter β in Eq. (3) should then be given by

$$\beta = T/2T_v . \quad (39)$$

The relaxation measurements in Fig. 1 find that β is about 0.6 at 500 K, which is reasonably consistent with the experimentally measured slope of the valence-band tail of 500 K. We note, however, that β is larger in doped *a*-Si:H, even though the valence-band tail is not correspondingly sharper.

An interesting feature of the model is that the energy to form mobile hydrogen interstitials (1.5 eV above the Si—H bonds) is close to the equivalent position of the valence-band-mobility edge ($E_D-0.7$ eV; see Fig. 5), when the doubling of the energy scale is included. We are unsure whether or not this is a coincidence. There is a general similarity in the two energies, because they cor-

respond to a density of states where the hydrogen (or band-edge holes) can diffuse from site to site without activation. This can presumably only occur when the density of states is of order a^{-3}, where a is the mean free path. Thus if both mean free paths are one or two bond lengths, then the density of states at the onset energy for mobile holes or mobile hydrogen will be similar.

Light-induced defects are found to anneal faster than the thermal defects by about an order of magnitude. The difference is that the optically induced defects are not necessarily in thermal equilibrium, and can include states of high formation energy. We assume that defect formation occurs when an electron-hole pair recombines and the energy released causes a hydrogen atom to be excited to a mobile state. The hydrogen will diffuse away and subsequently be trapped by a weak bond, creating defects by the mechanism of model 3. The defect density is expected to be proportional to the density of available states, $G_H(E)$, provided the temperature is low enough that the hydrogen is not reexcited. Most defects will be created with large formation energies because the density of such weak bonds is the greatest, as is schematically shown in Fig. 13. The faster annealing rate implies a correlation between the formation energy and the anneal energy, and this is provided by the hydrogen bonding model. The hydrogen in the higher-energy sites can diffuse more easily as the temperature is raised, and so the annealing rate will be correspondingly faster.

This model of hydrogen bonding and diffusion also predicts a connection between the defect density and the relaxation time, such that the sample with the highest defect density should have the longest equilibration time. A larger defect density is associated with a broader valence-band-tail state. Thus, in turn, leads to a broader distribution of hydrogen bonding energies, because of the correspondence between the valence-band tail and the hydrogen distribution. The hydrogen diffusion rate is reduced by the presence of the extra deep hydrogen traps, giving a slower relaxation. Our measurements shown in Fig. 4 find that the relaxation times increase with rf power during deposition. A high rf power also causes an increase in the defect density, and so is consistent with the hydrogen bonding model. Further experiments are needed to test whether this prediction is true for a wider set of deposition conditions.

V. CONCLUSIONS

The ESR experiments reported here provide further confirmation that the paramagnetic defects in a-Si:H are in thermal equilibrium with the band tails, with a temperature-dependent defect density. Equilibration is observed between 180 and 400 °C, with a reversible change in defect density of up to a factor 4. The relaxation towards equilibrium follows a stretched exponential form, and is thermally activated with an energy of about 1.5 eV. The actual relaxation time depends on the deposition conditions of the films.

A detailed analysis is made of the thermodynamics of the creation of neutral defects from weak bonds, for a number of specific defect reactions. Two of the models are similar to those considered earlier, and we also analyze models in which the motion of bonded hydrogen is specifically included. The calculations include the effect of a distribution of defect-gap-state energies. We conclude that all the models account for the weak temperature dependence of the defect density seen in the experimental data. It is argued that the defect reactions that do not involve hydrogen may not be physically possible, and instead we propose that one of the hydrogen-related models is the origin of the equilibration. Both models of this type give reasonable quantitative agreement with the data, for parameters that are consistent with experiment.

Our measurements confirm that the relaxation times are faster for light-induced defects than for thermally induced defects. A model is proposed to explain the result based on the distribution of defect-formation energies. We also propose that the distribution of hydrogen binding energies is closely related to that of the defect formation energies, and predict that the relaxation rates and defect densities should be correlated.

ACKNOWLEDGMENTS

The authors are very grateful for discussions with W. Jackson, Z. Smith, and M. Stutzmann, and for sample preparation by C. C. Tsai and R. Thompson. The research was supported by the Solar Energy Research Institute (Golden, CO).

[1]Z. Smith, S. Aljishi, D. Slobodin, V. Chu, S. Wagner, P. M. Lenahan, R. R. Arya, and M. S. Bennett, Phys. Rev. Lett. **57**, 2450 (1986).

[2]R. A. Street, J. Kakalios, and T. M. Hayes, Phys. Rev. B **34**, 3030 (1986).

[3]R. A. Street, J. Kakalios, C. C. Tsai, and T. M. Hayes, Phys. Rev. B **35**, 1316 (1987).

[4]R. A. Street, M. Hack, and W. B. Jackson, Phys. Rev. B **37**, 4209 (1988).

[5]T. J. McMahon and R. Tsu, Appl. Phys. Lett. **51**, 412 (1987).

[6]X. Xu, A. Morimoto, M. Kumeda, and T. Shimizu, Appl. Phys. Lett. **52**, 622 (1988).

[7]X. Xu, A. Okumura, A. Morimoto, M. Kumeda, and T. Shimizu, Phys. Rev. B **38**, 8371 (1988).

[8]C. Lee, W. D. Ohlsen, and P. C. Taylor, Phys. Rev. B **36**, 2965 (1987).

[9]Z. Smith and S. Wagner, Phys. Rev. Lett. **59**, 688 (1987).

[10]J. Kakalios, R. A. Street, and W. B. Jackson, Phys. Rev. Lett. **59**, 1037 (1987).

[11]R. A. Street, C. C. Tasi, J. Kakalios, and W. B. Jackson, Philos. Mag. B **56**, 305 (1987).

[12]J. Kakalios, R. A. Street, C. C. Tsai, and R. Weisfield, in *Amorphous Silicon Semiconductor—Pure and Hydrogenated,* MRS Symp. Proc. No. 95, edited by A. Madan, M. Thompson, D. Adler, and Y. Hamakawa (MRS, Pittsburgh, 1987), p. 243.

[13]W. B. Jackson and J. Kakalios, Phys. Rev. B **37**, 1020 (1988).

[14]G. Muller, S. Kalbitzer, and H. Mannsperger, Appl. Phys. A **39**, 243 (1986).

[15]G. Muller, Appl. Phys. A **45**, 103 (1988).

[16]Y. Bar-Yam, D. Adler, and J. D. Joannopoulos, Phys. Rev. Lett. **57**, 467 (1986).
[17]M. Stutzmann, Philos. Mag. B **56**, 63 (1987).
[18]V. Heine, in *Solid State Physics,* edited by H. Ehrenreich, F. Seitz, and D. Turnbull (Academic, New York, 1980), Chap. 1, p. 188.
[19]J. M. Marshall, R. A. Street, and M. J. Thompson, Phys. Rev. B **29**, 2331 (1984).
[20]K. Winer, I. Hirabayashi, and L. Ley, Phys. Rev. B **38**, 7680 (1988).
[21]C. D. Cody, T. Tieje, B. Abelès, B. Brooks, and Y. Goldstein, Phys. Rev. Lett. **47**, 1480 (1981).
[22]S. Pantelides, Phys. Rev. Lett. **58**, 3479 (1987).
[23]Z. Smith and S. Wagner, in *Advances in Amorphous Semiconductors,* edited by H. Fritzsche (World Scientific, Singapore, 1989), p. 469.
[24]R. Meaudre, P. Jensen, and M. Meaudre, Phys. Rev. B **38**, 12 449 (1988).
[25]R. A. Street, Solar Cells **24**, 211 (1988).
[26]W. B. Jackson and J. Kakalios, in *Advances in Amorphous Semiconductors,* Ref. 23, p. 247.
[27]W. B. Jackson and N. M. Amer, J. Phys. (Paris) Colloq. **42**, C4-293 (1981).
[28]M. Stutzmann, Philos. Mag. (to be published).